Properties of Spin and Fluorescent Labels at a Receptor-Ligand Interface

Rikard Owenius,* Maria Österlund,# Mikael Lindgren,* Magdalena Svensson,# Ole H. Olsen,§ Egon Persson,¶ Per-Ola Freskgård,¶ and Uno Carlsson#

*IFM-Department of Chemical Physics and #IFM-Department of Chemistry, Linköping University, SE-581 83 Linköping, Sweden; and §Medicinal Chemistry Research IV and ¶Tissue Factor/Factor VII Research, Novo Nordisk A/S, Novo Nordisk Park, Måløv, Denmark

ABSTRACT Site-directed labeling was used to obtain local information on the binding interface in a receptor-ligand complex. As a model we have chosen the specific association of the extracellular part of tissue factor (sTF) and factor VIIa (FVIIa), the primary initiator of the blood coagulation cascade. Different spectroscopic labels were covalently attached to an engineered cysteine in position 140 in sTF, a position normally occupied by a Phe residue previously characterized as an important contributor to the sTF:FVIIa interaction. Two spin labels, IPSL [N-(1-oxyl-2,2,5,5-tetramethyl-3-pyrrolidinyl)iodoacetamide] and MTSSL [(1-oxyl-2,2,5,5-tetramethylpyrroline-3-methyl)methanethiosulfonate], and two fluorescent labels, IAEDANS [5-((((2-iodoacetyl)amino) ethyl)amino)naphthalene-1-sulfonic acid] and BADAN [6-bromoacetyl-2-dimethylaminonaphthalene], were used. Spectral data from electron paramagnetic resonance (EPR) and fluorescence spectroscopy showed a substantial change in the local environment of all labels when the sTF:FVIIa complex was formed. However, the interaction was probed differently by each label and these differences in spectral appearance could be attributed to differences in label properties such as size, polarity, and/or flexibility. Accordingly, molecular modeling data suggest that the most favorable orientations are unique for each label. Furthermore, line-shape simulations of EPR spectra and calculations based on fluorescence depolarization measurements provided additional details of the local environment of the labels, thereby confirming a tight protein-protein interaction between FVIIa and sTF when the complex is formed. The tightness of this local interaction is similar to that seen in the interior of globular proteins.

INTRODUCTION

A fundamental property of all biological macromolecules is their ability to form noncovalent complexes of high affinity and specificity. It is through specific interactions that proteins recognize other molecules, such as nucleic acids, polysaccharides, lipid membranes, or other proteins, and spontaneously assemble into functional complexes with stable structures. Such protein-protein interactions are intrinsic to virtually every cellular process and have been shown to be an important aspect of the biological activity of a variety of different proteins, including transcription factors, immunoglobulins, cytokines, and receptors.

X-ray crystallography is a commonly used technique to obtain high-resolution structures of interacting proteins that has helped to significantly increase the knowledge concerning the global structure, but also regarding individual residues that may be important for protein stability and function. NMR methods can also be used to obtain highly detailed structures of proteins, but is still restricted to relatively small proteins. Furthermore, circular dichroism (CD) measurements can monitor conformational changes induced by protein-protein interaction, although not with high structural resolution.

Received for publication 20 April 1999 and in final form 17 July 1999.

Address reprint requests to Dr. Uno Carlsson, IFM-Department of Chemistry, Linköping University, SE-581 83 Linköping, Sweden. Tel.: +46 13281714; Fax: +46 13281399; E-mail: ucn@ifm.liu.se.

R. Owenius and M. Österlund contributed equally to this study.

0006-3495/99/10/2237/14 $2.00

An alternative technique that can provide structural information is to specifically introduce reporter groups, such as fluorescent or spin labels, into the proteins of interest (Likhtenshtein, 1993; Hubbell et al., 1998). This site-directed labeling approach is particularly applicable to proteins that can neither be analyzed by NMR spectroscopy nor crystallized successfully, e.g., membrane proteins. It involves introduction of a cysteine residue at a desired position in the protein, followed by attachment of a sulfhydryl-specific spectroscopic label. Such labels are sensitive to their local environment and can therefore monitor changes that occur in close vicinity of the mutation site.

Previously, we have utilized site-directed labeling in folding studies of human carbonic anhydrase II (HCA II) (Lindgren et al., 1993, 1995; Svensson et al., 1995). Since the physical principles that govern the noncovalent protein-protein association are the same as for the self-assembly or folding of a single macromolecule, it should be possible to study the mechanism of protein-protein interaction by the same probing approach. Thus, we have shown that the interaction between HCA II and the chaperonin GroEL can be specifically mapped by site-directed spin labeling (Persson et al., 1999). In the present work, we apply this methodology on a receptor-ligand system, i.e., a specific protein-protein interaction, in an attempt to resolve the molecular interactions and conformational changes at a specific site upon complex formation.

As a model system we have chosen two proteins involved in the initiation of blood coagulation, the extracellular part of tissue factor (sTF for soluble TF) and the plasma protein factor VIIa (FVIIa). The understanding of this specific recognition is of great interest and relevance because of its

confirmed importance in several pathological states. The crystal structures of sTF (Harlos et al., 1994; Muller et al., 1994, 1996) and of sTF in complex with FVIIa (Banner et al., 1996) as well as mutational studies of the proteins (Gibbs et al., 1994; Ruf et al., 1994, 1995; Schullek et al., 1994; Kelley et al., 1995) have provided a detailed picture of the global structure of the complex. Upon association an extensive surface area is buried between the proteins with a very complex binding pattern.

The purposes of the present work are 1) to show that the interaction between sTF and FVIIa can be probed using different types of labels, 2) to explain how the properties of the labels influence the obtained spectral data, and 3) to relate this information to the preferred location and orientation of the labels within the complex according to molecular modeling. We have used sTF as a target for mutation and introduced a cysteine in position 140, as a handle for the spectroscopic labels, by the substitution Phe→Cys (Fig. 1). Phe-140 has been identified, both in the crystal structure and in biochemical studies, as one of the residues in direct contact with FVIIa in the complex, which makes the position suitable for this study. We have used four different spectroscopic labels, the spin labels IPSL [N-(1-oxyl-2,2,5,5-tetramethyl-3-pyrrolidinyl)iodoacetamide] and MTSSL [(1-oxyl-2,2,5,5-tetramethylpyrroline-3-methyl)methanethiosulfonate], and the fluorescent labels IAEDANS [5-((((2-iodoacetyl)amino)ethyl)amino)naphthalene-1-sulfonic acid] and BADAN [6-bromoacetyl-2-dimethylaminonaphthalene] (Fig. 2). The labels possess unique properties that make them sensitive to environmental changes, readily registered by electron paramagnetic resonance (EPR) and extrinsic fluorescence spectroscopy, respectively.

The local environment of a spin label is estimated from the line-shape of the obtained EPR spectrum, which is sensitive to the rotational motion of the spin label. A fluorescent label, however, monitors local changes in polarity, which are observed as shifts in the emission wavelength maximum and/or changes in intensity. Since the spectroscopic labels differ in length, volume, flexibility, and polarity they will each monitor the interaction between sTF and FVIIa differently. Thus, from this multi-probing approach it should be possible to extract complementary information about the local environment of the interface between the docked protein molecules. The use of different labels has the advantage that, in addition to revealing different changes of physicochemical properties upon protein-protein association, they can map local environmental characteristics at different distances from the attachment site. A multi-label screening can also guide the selection of an appropriate label most suitable for a specified purpose.

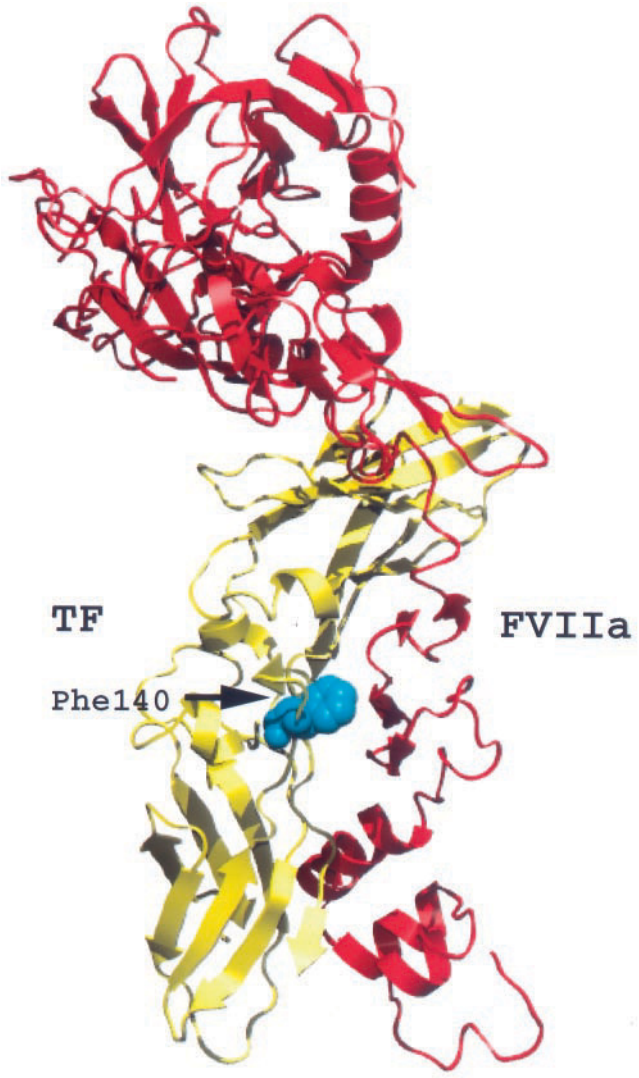

FIGURE 1 The structure of the sTF:FVIIa complex as determined by Banner et al. (1996). sTF is displayed in *yellow* and FVIIa in *red*. Position F140 (*blue, pointed out by the arrow*) is located in the β-hairpin intersection of the C-terminal domain of sTF within the buried surface area between the proteins.

MATERIALS AND METHODS

Chemicals

Isopropyl-β-D-thiogalactopyranoside (IPTG) was purchased from Promega (Madison, WI). The Ellman reagent 5,5′-dithiobis(2-nitrobenzoicacid) (DTNB) and the spin label N-(1-oxyl-2,2,5,5-tetramethyl-3-pyrrolidinyl)iodoacetamide (IPSL) were purchased from Sigma (St. Louis, MO). The spin label (1-oxyl-2,2,5,5-tetramethylpyrroline-3-methyl)methanethiosulfonate (MTSSL) was obtained from Reanal (Budapest, Hungary). The fluorescent labels 5-((((2-iodoacetyl)amino)ethyl)amino)naphthalene-1-sulfonic acid (1,5-IAEDANS) and 6-bromoacetyl-2-dimethylaminonaphthalene (BADAN) were obtained from Molecular Probes (Eugene, OR). The chromogenic substrate s-2288 was purchased from Chromogenix, Sweden. The isolation of human recombinant FVIIa and preparation of FVIIa affinity matrix have been described elsewhere (Thim et al., 1988; Freskgård et al., 1996). All other chemicals used were of analytical grade.

Spectrophotometers

Light absorption was measured on a Hitachi U-2000 instrument and the fluorescence measurements were performed on a Hitachi F-4500 spectrophotometer, supplemented with sheet polarizers for depolarization measurements.

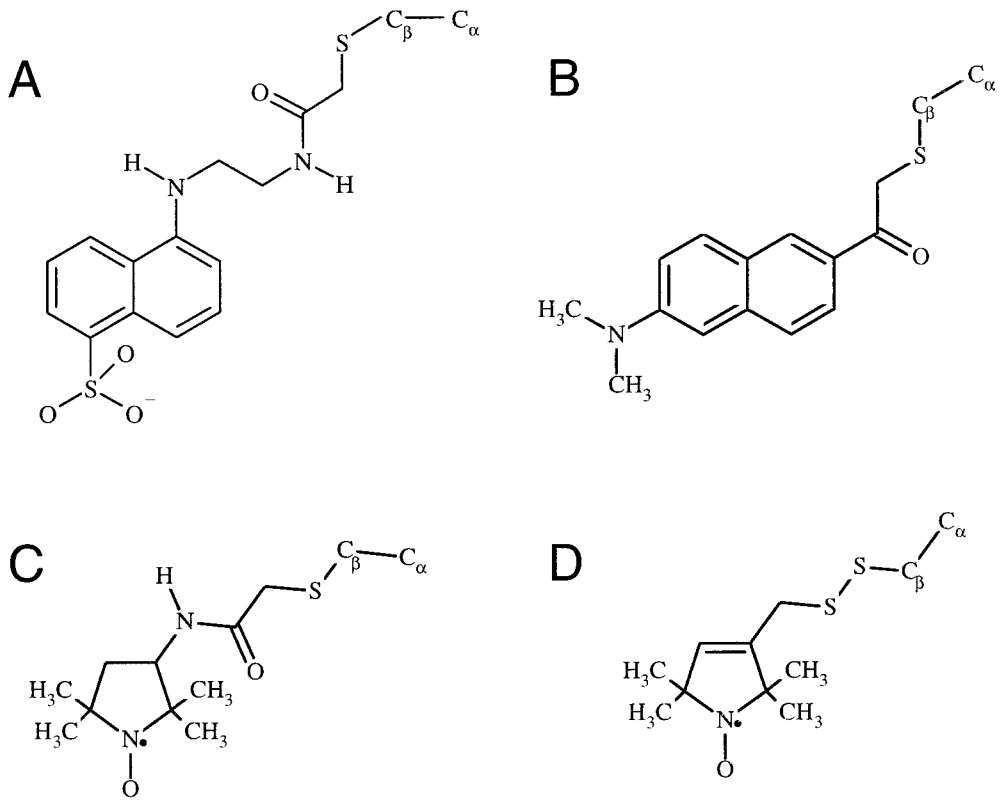

FIGURE 2 Structures of the four spectroscopic labels after reaction with a cysteine. (*A*) IAEDANS-labeled Cys, (*B*) BADAN-labeled Cys, (*C*) IPSL-labeled Cys, and (*D*) MTSSL-labeled Cys. The C_α, C_β, and S atoms of the cysteine are included to illustrate the length of the label from the backbone.

Protein isolation and purification

We used the QuikChange mutagenesis kit (Stratagene, La Jolla, CA) for the Phe→Cys mutation in position 140 of sTF (sTF(F140C)). sTF(F140C) was expressed and purified in *Escherichia coli* as described elsewhere (Stone et al., 1995; Freskgård et al., 1996) with some modifications. The cell lysis was performed by the X-press (Biox, Sweden) technique in 10 mM Tris-HCl buffer, pH 7.5, and thereafter resuspended in the same buffer with the addition of 1 mg DNAse. The solution was centrifuged at 11000 × *g* for 20 min at 4°C, and the inclusion bodies were denatured in 75 ml 6 M GuHCl, 0.5 M NaCl, and 20 mM Tris-HCl, pH 8.0. Refolding was achieved after 1 h incubation at room temperature by dropwise diluting the denatured protein into a 1 L solution containing 50 mM Tris-HCl, 0.25 M NaCl, pH 8.0 during gentle stirring for ~2 h. Purification was performed using Q-Sepharose Fast Flow (Pharmacia, Uppsala, Sweden) and FVIIa affinity chromatography as described by Freskgård et al. (1996). sTF(F140C) was then concentrated in a Centricon-10 (Amicon Inc., Beverly, MA) and buffered with 50 mM Hepes, 150 mM NaCl, pH 7.5. This buffer was then used in all subsequent measurements. The homogeneity of the protein was verified by SDS-PAGE. The concentration was measured at A_{280nm} and determined using a calculated extinction coefficient of 37440 M^{-1} cm^{-1} (Gill and von Hippel, 1989).

Labeling with spectroscopic labels

The labeling was carried out in the dark for several hours at 23°C using a 10-fold molar excess of label over sTF(F140C) in 0.1 M Tris-HCl, pH 8.0. Excess label was removed by dialysis against the buffer used for the FVIIa affinity column: 50 mM Tris-HCl, 10 mM $CaCl_2$, pH 8.0. After modification the affinity chromatographic purification was performed to assure a native conformation of the labeled protein in the subsequent measurements. The degree of IAEDANS and BADAN labeling was determined by measuring the absorbance at 336 nm and 387 nm using the extinction coefficients 5700 and 21,000 M^{-1} cm^{-1}, respectively. For the degree of IPSL and MTSSL labeling, an aliquot of the solution was withdrawn and DTNB was added in a 10-fold molar excess followed by spectrophotometric determination of free thiol groups at 412 nm, using $\epsilon_{412nm} = 14150$ M^{-1} cm^{-1} (Riddles et al., 1983).

Activity measurements

To determine the ability of the sTF variants to promote FVIIa activity, an amidolytic assay was performed as described by Persson et al. (1997). Briefly, 10 nM FVIIa was titrated with various concentrations (0–500 nM) of the sTF variants in 50 mM Hepes, 150 mM NaCl, 5 mM $CaCl_2$, pH 7.5.

Circular dichroism (CD) measurements

CD spectra were collected at 23°C in both near-UV (260–320 nm) and far-UV (180–260 nm) on a CD6 spectrodichrograph (Jobin-Yvon Instruments, Longjumeau, France). CD measurements were performed on the unlabeled and labeled sTF(F140C) as well as the wild-type sTF in 10 mM phosphate buffer, pH 7.5 at a protein concentration of 0.3–0.5 mg/ml. A 1-mm and a 0.5-cm pathlength were used in the near- and far-UV wavelength region, respectively. The observed ellipticities were converted to mean residue ellipticities [Θ] based upon a molecular weight of 25,000 and 219 amino acid residues.

Fluorescence measurements

Fluorescence emission spectra were recorded for sTF(F140C) labeled with either IAEDANS or BADAN at 400–600 nm after excitation at 350 and

380 nm, respectively. All measurements were performed in a 0.5-cm quartz cell with the cell compartment maintained at 23°C. A spectrum was recorded with labeled sTF(F140C) in 50 mM Hepes, 150 mM NaCl, pH 7.5. After addition of FVIIa in a 1.5-fold molar excess over labeled sTF(F140C) with a final $CaCl_2$ concentration of 5 mM, another spectrum was recorded. The concentration of labeled sTF(F140C) was held at 1–2 μM for all samples with a 5-nm bandwidth for excitation and emission. For quantum yield studies the wavelength-dependent sensitivity of the instrument was recorded with an optically dense solution of rhodamine B in a triangular cuvette acting as a quantum counter. The relative fluorescence quantum yield of the sTF(F140C)-IAEDANS was measured against IAEDANS-labeled β-mercaptoethanol. Fluorescence spectra were recorded with vertically polarized light and the emission polarizer in magic angle to vertical position. The fluorescence lifetime was calculated from the relative fluorescence quantum yield and the reported fluorescence lifetime for IAEDANS-labeled β-mercaptoethanol ($\tau = 15$ ns) (Cantor and Schimmel, 1980). The emission anisotropy was calculated from

$$r_s = \frac{F_{VV} - GF_{VH}}{F_{VV} + 2GF_{VH}}$$

where the subscripts refer to vertical or horizontal settings of the excitation and emission polarizers, respectively. The correction factor $G = F_{HV}/F_{HH}$ compensates for the unequal transmission efficiencies of vertically and horizontally polarized light.

Fluorescence emission spectra of fluorophore-labeled β-mercaptoethanol at various ratios of ethanol/water were also obtained to investigate the sensitivity of the fluorescent labels. These reference samples were prepared by allowing solutions of IAEDANS and BADAN to react with β-mercaptoethanol in 0–50% ethanol following the same procedure as the labeling of sTF(F140C). Measurements were performed as described for labeled protein but with a label concentration of 8 μM and bandwidths for excitation and emission of 5 and 2.5 nm, respectively. The fluorescence emission of the samples was recorded and maximum wavelength and fluorescence intensity were compared for the two labels.

EPR measurements

EPR measurements were carried out using a Bruker CW X-band spectrometer consisting of a combination of the ER200D-SRC and ESP300 systems. An ER4103TM cavity connected to the 200 mW microwave bridge was used for measurements at room temperature. The different protein samples were introduced in a standard TM_{110} flat cell for aqueous samples (Wilmad Glass, Buena, NJ). EPR spectra were acquired from sTF(F140C) labeled with either IPSL or MTSSL in 50 mM Hepes, 150 mM NaCl, pH 7.5. Then, FVIIa was added in a 1.5-fold molar excess over sTF(F140C) with a final $CaCl_2$ concentration of 5 mM, followed by recording of spectra. All measurements were performed under equilibrium conditions. The sTF(F140C) concentration was 5–7 μM. All experiments on protein solutions were performed at room temperature (20 ± 1°C).

The isotropic (g_{iso}, A_{iso}) and anisotropic (g_{zz}, A_{zz}) parameters were obtained for IPSL and MTSSL located in either a polar (Tris-HCl) or hydrophobic (octanol) environment. The spin labels were allowed to react with a 1.5-fold molar excess of β-mercaptoethanol in either 0.1 M Tris-HCl, pH 7.5 or 99% octanol in the dark for several hours at room temperature. The final spin label concentration was 16 μM (in Tris-HCl) or 32 μM (in octanol). Isotropic parameters (g_{iso}, A_{iso}) were obtained from a series of samples by recording spectra at room temperature using the same set-up as for the protein samples. Another series of samples was transferred to 4-mm quartz tubes (Wilmad Glass) and were then frozen under evacuation using liquid nitrogen to 77 K. Each sample was frozen (after the sample tube had been evacuated to 0.05–0.1 torr) and thawed three times directly followed by a final freezing to reduce the amount of oxygen dissolved in the frozen sample. The measurements were made at 77 K using a standard EPR liquid nitrogen dewar (Wilmad Glass) employing the outer cavity of a 9201dr350 double resonator (Bruker), from which the anisotropic parameters (g_{zz}, A_{zz}) were read directly from the spectra. Error estimates of g_{iso}, A_{iso}, g_{zz}, and A_{zz} were determined by re-analyzing recorded spectra and re-measuring at least two samples prepared at different occasions (errors included in Table 4). With maximum error we here mean the largest deviation from the parameter values as given in Table 4. The onset of saturation of the EPR signal of the frozen spin label/solvents was found to occur between ~0.1 and 0.5 mW of microwave power.

Line-shape distortions that could arise from experimental conditions such as overmodulation or microwave saturation were avoided by setting the modulation amplitude lower than one-half of the linewidth of the $m_I = 0$ nitrogen hyperfine transition, and by recording the EPR spectra at 4 mW (room temperature) or 0.1–0.2 mW (77 K) microwave power. All first-derivative EPR spectra were baseline-corrected and normalized to a constant spin concentration (Bruker Win-EPR 2.11 and Matlab 5.2).

EPR line-shape simulations

To analyze EPR spectra and estimate the dynamic parameters of the spin labels in the various protein configurations, the published simulation program developed by Freed and co-workers was used (Schneider and Freed, 1989), specifically the LBLL, EPRLL programs, and associated subroutines. The subroutines were merged into one Fortran program making minimal changes to the original Fortran 77 code carrying out the actual line-shape calculation. Subroutines were compiled and linked using MS Fortran Powerstation 4.0 in an NT 4.0 (200 MHz) or Win98 environment (450 MHz). Each spectrum took ~10–30 s to calculate depending on the basis set appropriate for the diffusion model (see Schneider and Freed, 1989).

The following parameters were considered when calculating and adjusting the EPR line-shape of the nitroxide radicals to experimental data: the anisotropic hyperfine tensor [A_{xx}, A_{yy}, A_{zz}] and g tensor [g_{xx}, g_{yy}, g_{zz}]; the axially symmetric Brownian diffusion tensor [d_{xy}, d_{zz}] whose frame of rotation is related to the magnetic frame through the diffusion tilt angle; and finally, the intrinsic (Lorentzian) line-width (lw) and Gaussian (convoluted) line-width (gw). The rotational diffusion tensor elements d_{xy}, d_{zz}, are often referred to as $R_\perp$ and $R_\parallel$, respectively. The meaning of the coordinate axis system and relation between molecular magnetic and diffusion frame is depicted in Fig. 2 in Schneider and Freed, 1989. The isotropic hyperfine splitting and g value (A_{iso}, g_{iso}) were obtained from measurements of IPSL and MTSSL under conditions where the labels are tumbling freely on the EPR time-scale. Furthermore, the rigid-state hyperfine splitting and g value (A_{zz}, g_{zz}) associated with the magnetic field along the π orbital of the unpaired electron, usually defined as the z axis, were obtained by performing measurements at cryogenic temperatures. In this way, the search for the model describing the local dynamic structure of the labels is considerably simplified. The parameters obtained from a spin label in the polar solvent were then used as start values in the simulation of spectra from spin-labeled sTF(F140C), since the label is expected to be solvent-exposed, i.e., in a polar environment. The parameters from a label in the apolar environment were used as start values in the simulation of spectra from spin-labeled sTF(F140C):FVIIa, where the label is believed to be in a hydrophobic environment. The search for simulated spectra best fitting the experimental ones was performed by first adjusting isotropic rotational diffusion parameters assuming axial symmetry, i.e., $g_{xx} = g_{yy}$ and $A_{xx} = A_{yy}$ (these become uniquely defined by the constraints set by the isotropic parameters and the axial components). The simulations were then further refined by adding a rhombic distortion to the magnetic parameters, varying the line-width, and assuming axial symmetric diffusion parameters (if necessary) and varying the diffusion tilt parameter (Schneider and Freed, 1989). In the final step A_{zz} and g_{zz} were also allowed to vary.

It is difficult to estimate the error of each individual tensor component since these to varying degree contribute to the apparent line-shape for a particular dynamic model and overall motion. A rough error estimate can be based on the "best-fit" between experimental and simulated spectra as presented in Fig. 5. Thus, varying either $A_{ii} = \pm 0.2$ G, $g_{ii} = \pm 0.0002$, or $d_{ii} = \pm 5\%$ gives a substantially different simulation if the parameter in question is critical. This estimate is based on a comparison of at least 50 simulated spectra for each case.

The files generated by the Fortran program were used as input to Matlab 5.2 and programs based on Matlab standard routines were made that allowed for further postprocessing. The postprocessing included convolution with a Gaussian line-shape to obtain the Gaussian line-width parameter (accounts for the unresolved hyperfine splitting from hydrogens within the spin label), normalization, automatic fitting routines for spectra decomposition, and presentation of simulated and experimental data. The Gaussian line-width was determined from simulations of spectra recorded near the "free rotation limit," and retained constant in all simulations.

Modeling of label properties

The structural properties of the spectroscopic labels were determined using data from the molecular modeling of the labeled sTF:FVIIa complex starting from the crystallographic coordinates (1DAN) and using the Sybyl software from Tripos Inc. on a Silicon Graphics O_2 workstation. Label volumes were determined from molecular surfaces (Connolly, 1983) obtained from energy minimized molecular models of each label attached to a cysteine (QUICK MINIMIZE routine in Sybyl). Lipophilicity potentials (LP) describing the hydrophobic properties of the labels were determined from the same molecular surfaces according to Heiden et al. (1993).

Molecular modeling

To explore possible modes of interaction between the inserted label and protein(s), a systematic adiabatic approach was pursued which evaluates a discrete set of label side-chain conformations. The side-chain conformations were generated by constraining the torsional angles of the label to a discrete set of likely conformers. No solvent molecules were taken into account. Further, it was assumed that the hydrophobic character of the labels promotes protein interaction. Therefore, only label conformations that interact favorably with the protein were considered.

Topology templates of the four labels were built in Quanta (Molecular Modeling Software, Release 3.3, 1992, Molecular Simulations Inc., Waltham, MA). To elucidate the conformation of the nitroxide group in IPSL and MTSSL a quantum mechanical geometry optimization was performed (SPARTAN 5.0, Wavefunction Inc., Irvine, CA) which predicts a planarity of the atomic arrangement of the nitroxide ring moiety. The molecular mechanical calculations were performed within the framework of the CHARMM22 modeling package (Brooks et al., 1983) using an all-hydrogen approach (as described in the template file AMINOH.RTF). Side-chain conformations were systematically analyzed by successively constraining all torsional angles for C–C and C–S bonds to 180, 60, and $-60°$, and S–S bonds to 90 and $-90°$ while keeping peptide bonds in *trans* conformation. Thus, e.g., for MTSSL, $3 \times 3 \times 3 \times 3 \times 3 = 243$ conformations were considered. Other cases are summarized in Table 1. Each conformation was constructed using torsional harmonic potentials with spring constants of 1000 kcal/mol. After energy minimization (using a steepest descent (SD) method (250 steps) followed by an adopted basis Newton Raphson (ABNR) method (250 steps) with a distance-dependent dielectric ($\epsilon_0 = 10$)), the van der Waals (vdW) interaction energy between the side chain in question and protein, as well as the total vdW energy, was evaluated to exclude side-chain conformations that clash with protein. If the total vdW energy as well as the interaction between the side chain and protein were negative, all atoms closer than 6 Å from a label atom were further energy-minimized (75 steps of SD followed by 75 steps of ABNR). If the resulting vdW interaction energy was <-30 kcal/mol, the structure was saved for further analysis. From Table 1 it is seen that ~50% of the tested structures were accepted due to a favorable interaction energy.

TABLE 1 Label conformations considered in molecular modeling

Label*	Number of conformations	Accepted conformations
IAEDANS	8748	3815 (44%)
BADAN	324	123 (38%)
IPSL	162	84 (52%)
MTSSL	243	118 (49%)

*Labels are attached to Cys at position 140.

RESULTS

Protein preparation

Recombinant sTF is obtained as inclusion bodies. Since native sTF contains two disulfide bridges, denaturation of the inclusion bodies is performed under reducing conditions from which the native disulfides can successfully be regained with a high yield upon refolding (Freskgård et al., 1996). However, by following this purification protocol for the sTF(F140C) mutant only very low yield of active protein was obtained. This problem is probably related to the introduction of an extra cysteine in the protein. Although the engineered cysteine is located far away from any of the native cysteines in the primary as well as in the tertiary structure, it is likely to interfere with the native cysteines during the in vitro folding process, thereby forming incorrect internal disulfide bridges. These complications were overcome by omitting reducing agents during denaturation and refolding of the inclusion bodies. Hence, the protein in the inclusion bodies possesses native cystines and the inserted cysteine is not engaged in intermolecular disulfide bridges to any great extent. By using this procedure, more than a 10-fold increase in the yield of sTF(F140C) was achieved. A 3-L culture yielded ~50 mg of pure protein.

Characterization of the unlabeled and labeled sTF(F140C)

The purity of the protein was verified by SDS-PAGE (not shown). CD measurements on sTF(F140C) were performed to control the conformational integrity. The resemblance of the CD spectra of the wild-type sTF and sTF(F140C) was very close (data not shown). sTF causes allosteric changes in FVIIa that enhance amidolytic activity. Normal binding is demonstrated by the sTF-dependent enhancement of the FVIIa amidolytic function. The ability of sTF(F140C) to activate FVIIa was only slightly decreased as a result of the mutation (Table 2).

It was possible to achieve almost complete labeling (>95%) of the –SH moiety in position 140 with all spec-

TABLE 2 Amidolytic activity of FVIIa

sTF Variant*	Activity# (%)
wt	100.0
F140C	83.6
IAEDANS	86.0
BADAN	84.7
IPSL	89.3
MTSSL	74.9

*Labels are attached to Cys at position 140.
#Maximal stimulation of FVIIa activity by sTF variants.

troscopic labels used. All the labeled sTF(F140C) variants stimulated the amidolytic activity of FVIIa similarly to sTF(F140C) (Table 2). Conformational changes in sTF by the labeling was investigated using CD. In agreement with the functional assay, no major differences were observed between the wild-type and the labeled variants of sTF. These data demonstrate that sTF(F140C) and the labeled variants appear to be structurally similar to the wild-type sTF.

Characterization of labels

To evaluate the important properties of a spectroscopic label that determine its probing function, it is necessary to isolate the parameters that are most likely responsible for the behavior of the label. Structures of the different labels are shown in Fig. 2 and selected parameters are presented in Table 3. All four labeled side chains occupy a much larger volume than the wild-type Phe or engineered Cys. There is also a notable difference between the labels themselves, both regarding structure and size. IAEDANS is the largest, BADAN and IPSL are slightly smaller, and MTSSL is the smallest of the labels. Furthermore, by determining the extreme lipophilicity potentials of the labels, it was apparent that the hydrophobic properties of the labels varied considerably (Table 3). These data showed that BADAN has a more hydrophobic character than IAEDANS and that IPSL is mainly hydrophilic, whereas MTSSL possesses both hydrophilic and hydrophobic characters. Furthermore, the flexibility of the labels differs due to different covalent bonds to the engineered cysteine in sTF and different numbers and types of bonds in the linker, i.e., the atoms between the sulfur of the cysteine and the fluorophore or nitroxide ring (Fig. 2).

To investigate the response of the fluorophore labels toward polarity changes, fluorescence emission spectra were recorded in various concentrations of ethanol. Even though the fluorescent labels have different properties (Table 3), their sensitivity to changes in polarity is similar, as judged from changes in wavelength maximum (Fig. 3). However, the increase in fluorescence intensity is more pronounced for BADAN compared to IAEDANS when exposed to an apolar environment (Fig. 3). Moreover, indications of a solvent dependency were also found among the EPR parameters obtained for IPSL and MTSSL in Tris-HCl and octanol at room and cryogenic temperatures (Table 4). Both hyperfine splitting constants (A_{iso}, A_{zz}) are smaller for IPSL and MTSSL in a nonpolar solvent compared to a polar one. A small difference was also noted for g_{iso} being slightly larger in the nonpolar solvent, while the change of g_{zz} was not significant. However, the shifts of the g values are considerably smaller than the shifts of the hyperfine splitting constants and are difficult to determine accurately from line-shape simulations.

Probing the sTF:FVIIa assembly with fluorescent labels

Fluorescence spectra of sTF(F140C) labeled with IAEDANS or BADAN are displayed in Fig. 4. These spectra show the fluorescence before and after the formation of the sTF(F140C):FVIIa complex. The IAEDANS-labeled mutant displayed a maximum fluorescence intensity at 497 nm, which upon mixing with FVIIa was blue-shifted to 487 nm. The fluorescence intensity increased ~55% upon association of FVIIa. For the BADAN-labeled mutant the fluorescence wavelength maximum shifted from 536 to 525 nm, whereas the intensity differed by <5%. Because the fluorescence spectra were equally blue-shifted (~10 nm) for the IAEDANS- and BADAN-labeled sTF(F140C) when complexed to FVIIa, both labels appear to probe an environment that is of the same polarity. From our model studies the measured emission maxima, when the complex is formed, corresponds to a milieu of the labels that is equivalent to the polarity of 45% ethanol in water. The corresponding spectra of the labeled sTF(F140C) variants not bound to FVIIa indicate an environment of the labels that is more polar (20% ethanol in water) (Fig. 3).

The fluorescence depolarization measurements for the uncomplexed form of IAEDANS-labeled sTF(F140C) re-

TABLE 3 Properties of the spectroscopic labels

Side Chain*	Probing Distance# (Å)	Volume§ (Å^3)	LP¶ Min Value	LP¶ Max Value
Phe	6.2	117.5	0.129	0.162
Cys	3.6	60.6	0.017	0.069
IAEDANS	8.7 ± 1.5	331.8	−0.024	0.034
BADAN	6.6 ± 1.0	274.3	0.042	0.099
IPSL	7.4 ± 1.2	277.9	−0.035	−0.003
MTSSL	7.1 ± 1.0	255.5	−0.021	0.010

*Either amino acid residue or label attached to Cys residue.

#Maximum length of Phe and Cys from the C_α obtained from energy-minimized models of the side chains (QUICK_MINIMIZE routine in Sybyl), or distance from C_α to the center of the fluorophore for IAEDANS and BADAN or the nitroxide nitrogen for IPSL and MTSSL determined from molecular modeling of the labels incorporated within the protein complex. The errors shown are standard deviations.

§Determined from a surface model made with a probe radius of 1.4 Å, i.e., corresponding to the surface accessible to a water molecule, as described in Materials and Methods.

¶Minimum and maximum values of the lipophilicity potential (LP) calculated for each side chain as described in Materials and Methods.

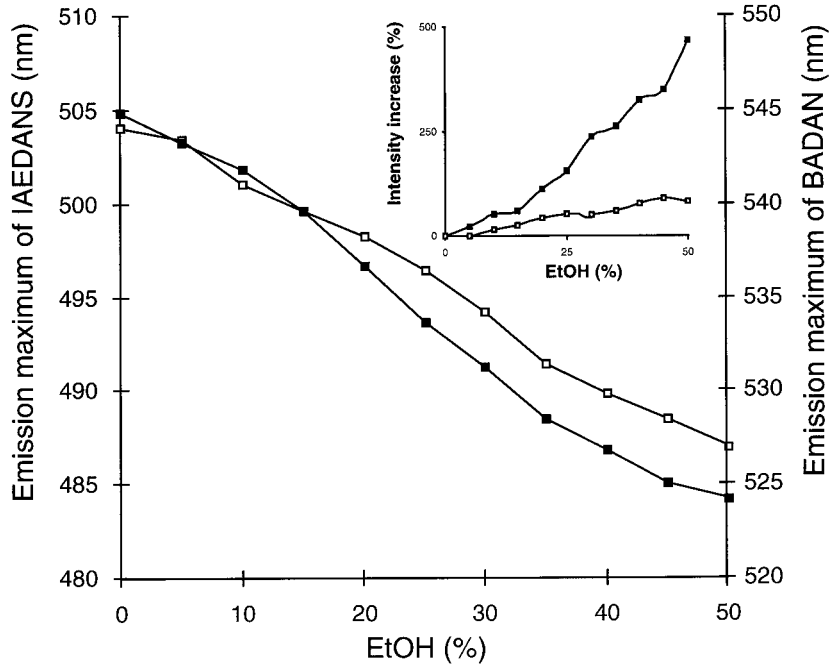

FIGURE 3 Emission wavelength maxima of the fluorescent labels, IAEDANS (□) and BADAN (■), linked to β-mercaptoethanol in various concentrations of ethanol. The *inset* shows the increase in intensity for the same measurements.

sulted in a relative quantum yield of 0.7 and an anisotropy of 0.06. The corresponding values for the sTF(F140C):FVIIa complex were 1.06 and 0.26, respectively. From the relative quantum yield and the reported fluorescence lifetime of IAEDANS-labeled β-mercaptoethanol the fluorescence lifetime of sTF(F140C)-IAEDANS could be calculated to be 15.9 ns in the complex with FVIIa. The overall rotational correlation time, ϕ_c, was calculated from the Perrin equation

$$r_s = \frac{2}{5(1 + \tau/\phi_c)}$$

and was found to be 35 ns. For an approximately spherical molecule this value was used to estimate the radius of the sTF:FVIIa complex from the Einstein-Stokes equation

$$\phi_c = \eta V/kT$$

where V is the molecular volume, η is the solvent viscosity, k the Boltzmann's constant, and T the temperature (20°C). The calculated radius of the protein complex was 33 Å. The fluorescence lifetime of BADAN was not long enough to enable any depolarization studies.

Probing the sTF:FVIIa assembly with spin labels

EPR spectra of the spin-labeled sTF(F140C) with or without FVIIa are presented in Fig. 5, where spectra of IPSL-labeled sTF(F140C) and spectra of MTSSL-labeled sTF(F140C) are shown in Fig. 5, *A* and *C*, respectively. There is a marked change in spectral appearance when FVIIa binds to spin-labeled sTF(F140C), regardless of spin label used (Fig. 5, *B* and *D*). Furthermore, there is an evident difference in shape of the acquired EPR spectra depending on whether sTF(F140C) is labeled with IPSL or MTSSL. The lineshape of the EPR spectrum is influenced by the mobility of the spin label, which is restricted by surrounding groups. The less mobile the spin label, the more contribution is seen from the anisotropic hyperfine interaction that results in a broadening of the spectral bands. Thus, by mere inspection it is apparent that MTSSL is less mobile than IPSL in the

TABLE 4 EPR parameters of MTSSL and IPSL attached to β-mercaptoethanol in various environments

	MTSSL		IPSL	
Parameter*	Polar environment#	Non-polar environment§	Polar environment#	Non-polar environment§
g_{iso}	2.00535	2.00564	2.00535	2.00565
A_{iso} (G)	16.27	15.03	16.00	14.80
g_{zz}	2.0021	2.0021	2.00215	2.00215
A_{zz} (G)	36.15	34.80	36.65	35.15

*Parameters are defined in Materials and Methods. g_{iso} and A_{iso} are obtained at room temperature (20 ± 1°C), g_{zz} and A_{zz} at 77 K. Errors: g_{iso} (±0.00005), A_{iso} (±0.05 G), g_{zz} (±0.00015), A_{zz} (±0.15 G).
#0.1 M Tris-HCl, pH 7.5.
§99% octanol.

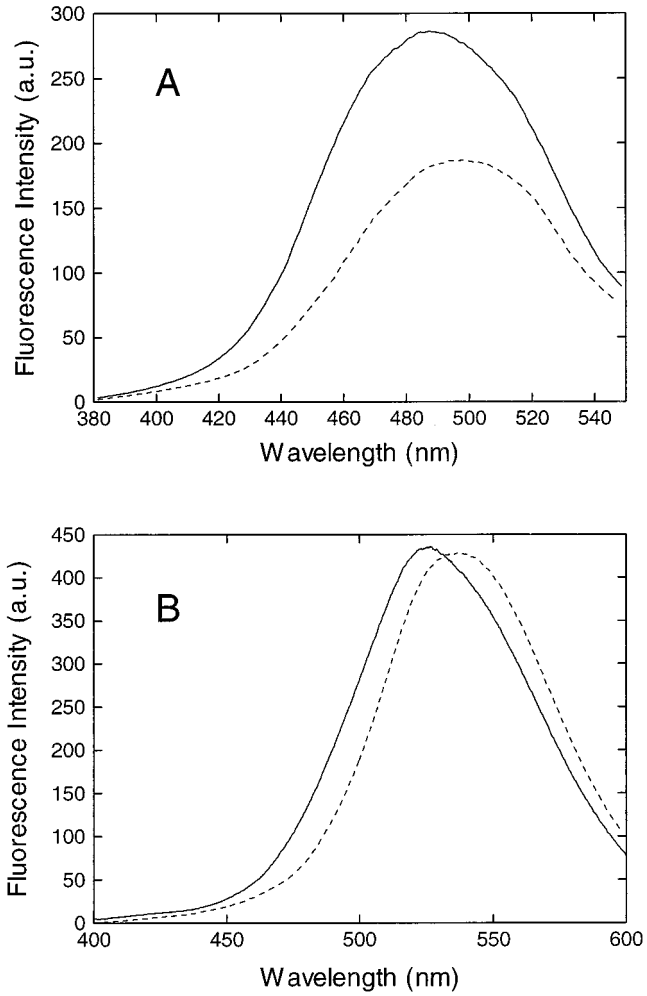

FIGURE 4 (*A*) The fluorescence emission spectra of IAEDANS-labeled sTF(F140C) (*dashed line*) and IAEDANS-labeled sTF(F140C) in complex with FVIIa (*solid line*). Excitation was performed at 350 nm. (*B*) The fluorescence emission spectra of BADAN-labeled sTF(F140C) (*dashed line*) and BADAN-labeled sTF(F140C) in complex with FVIIa (*solid line*). Excitation was performed at 380 nm.

uncomplexed sTF(F140C) and is also more immobilized when the sTF(F140C):FVIIa complex has formed.

Line-shape simulations revealed more details of the local dynamic structure surrounding the spin labels in sTF(F140C) and the changes accompanying complex formation. Simulated line-shapes are shown together with the experimental spectra in Fig. 5 with the detailed parameters used in the simulations summarized in Table 5. The simulated EPR spectra of sTF(F140C) labeled with IPSL or MTSSL show that both labels are rotating in an anisotropic environment (Fig. 5, *A* and *C*). The pronounced sharp central line with high amplitude relative to the low-field and high-field features can only be reproduced in simulations using an anisotropic rotational diffusion and a tilt angle of 20–40°. The "kink" on the low field side of the MTSSL spectrum could not be reproduced using a single component. The results for IPSL show a similar anisotropy of the motion, but with a two to six times faster dynamics. The spectrum obtained for IPSL-labeled sTF(F140C):FVIIa could be interpreted as a superposition of a slow and a faster component, the latter contributing ~20% (Fig. 5 *B*). In the case of MTSSL-labeled sTF(F140C):FVIIa the experimental spectrum was more well-defined and no fast component was needed to reproduce the line-shape (Fig. 5 *D*). The discrepancy between the calculated and experimental spectra in the vicinity of 3460 G might be due to a partially resolved dipolar hyperfine interaction to a hydrogen with its maximum hyperfine splitting along the high g-value orientation. This is a reasonable assumption in view of the slow motion of the complex, but could not be verified, since the program used for calculating the simulation only allows one anisotropic nucleus.

An interesting observation we made was that EPR is capable of revealing conformational heterogeneities in the spin-labeled sTF(F140C) sample that can not be detected by CD. Even a very small fraction of denatured or misfolded protein molecules appears clearly as a second species with notably sharp peaks in the EPR spectrum. The efficiency of the FVIIa affinity column for purification of sTF(F140C) was confirmed, since it completely removed any contribution of nonnative protein to the spectrum.

Molecular Modeling

Model building provides a rationale as to how the inserted labels may be situated in the interface between sTF and FVIIa, how the tether of the label may be constrained in finding its way from the backbone, and how the labels interfere with surrounding protein structure. The inserted labels (Fig. 2) were allowed to rotate about the side chain dihedral angles to search for low-energy conformation states in the sTF:FVIIa complex structure (see Materials and Methods for a detailed description). Fig. 6, *A–D* show the possible number of structures as a function of the calculated energies for each label. In all cases, the lowest energy conformation for each label was detected in, or close to, the cavity where the wild-type Phe is situated. The resulting subpopulation of structures was then used as the basis for the energy minimization where the neighboring region was allowed to adjust to accommodate the inserted labels. Fig. 7, *A–H* show the final orientation of each label compared with wild-type Phe. All labels except IAEDANS seem to occupy the same space as the wild-type Phe residue in the complex.

DISCUSSION

The strategy to use protein engineering to introduce spectroscopic labels into specific positions of the protein structure has been employed by us in earlier studies to probe local intramolecular conformational and environmental changes occurring during the folding process (Lindgren et al., 1993, 1995; Svensson et al., 1995, Hammarström et al., 1998). Furthermore, protein-protein interactions can be specifically mapped by this technique as shown for human

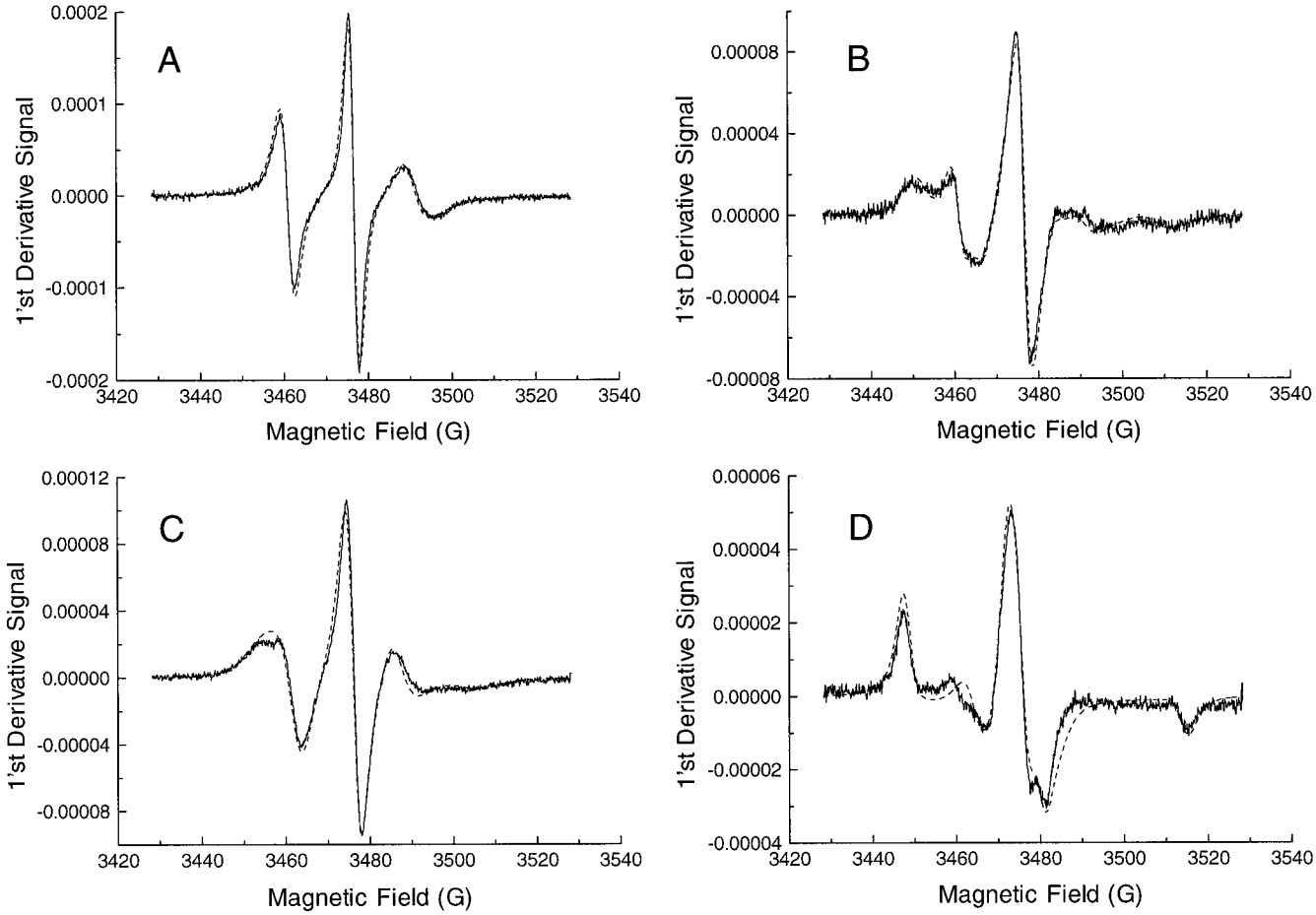

FIGURE 5 Experimental and simulated EPR spectra. (*A*) IPSL-labeled sTF(F140C), (*B*) IPSL-labeled sTF(F140C) in complex with FVIIa, (*C*) MTSSL-labeled sTF(F140C), and (*D*) MTSSL-labeled sTF(F140C) in complex with FVIIa. Experimental (*solid line*) and simulated (*dashed line*) EPR spectra. Hyperfine splitting and g-tensor components are given in Table 5.

carbonic anhydrase II (HCA II) and the chaperonin GroEL (Persson et al., 1999). In the present study, we have applied the site-directed labeling approach to a protein complex which relies on very specific protein-protein interactions, namely the receptor-ligand system sTF:FVIIa. This enzyme complex is considered to be responsible for the initiation of the blood clotting cascade (Mann et al., 1990; Davie et al., 1991).

sTF has a rigid structure that is virtually not changed during complex formation with FVIIa as inferred from a comparison of the crystal structure of free sTF (Harlos et al., 1994; Muller et al., 1994, 1996) with that of the sTF:FVIIa

TABLE 5 EPR parameters of MTSSL and IPSL attached to sTF(F140C)

	MTSSL[#]		IPSL[§]	
Parameter*	sTF(F140C)	sTF(F140C):FVIIa	sTF(F140C)	sTF(F140C):FVIIa
g_{iso}	2.0054	2.0054	2.0054	2.0054
A_{iso} (G)	16.2	15.9	16.0	15.7
A_{zz} (G)	35.5	34.7	35.9	35.0
d_{xy} (s^{-1})	$2.6 \cdot 10^7$	$1.5 \cdot 10^6$	$5.0 \cdot 10^7$	$1.8 \cdot 10^7$
d_{zz} (s^{-1})	$6.5 \cdot 10^8$	$1.5 \cdot 10^6$	$4.0 \cdot 10^9$	$1.8 \cdot 10^7$
Diffusion tilt	24°	—	25°	—
lw (G)	0.25	1.65	0.05	0.1
gw (G)	1.5	1.5	1.5	1.5

*Parameters are defined in Materials and Methods.

[#]Remaining EPR *g*- and hyperfine tensor components used in simulations of MTSSL spectra: $g_{xx} = 2.0080$, $g_{yy} = 2.0059$, $g_{zz} = 2.0023$, $A_{xx} = 7.1$ G, $A_{yy} = 6.0$ G.

[§]Remaining EPR *g*- and hyperfine tensor components used in simulations of IPSL spectra: $g_{xx} = 2.0084$, $g_{yy} = 2.0056$, $g_{zz} = 2.0022$, $A_{xx} = 6.5$ G, $A_{yy} = 5.5$ G.

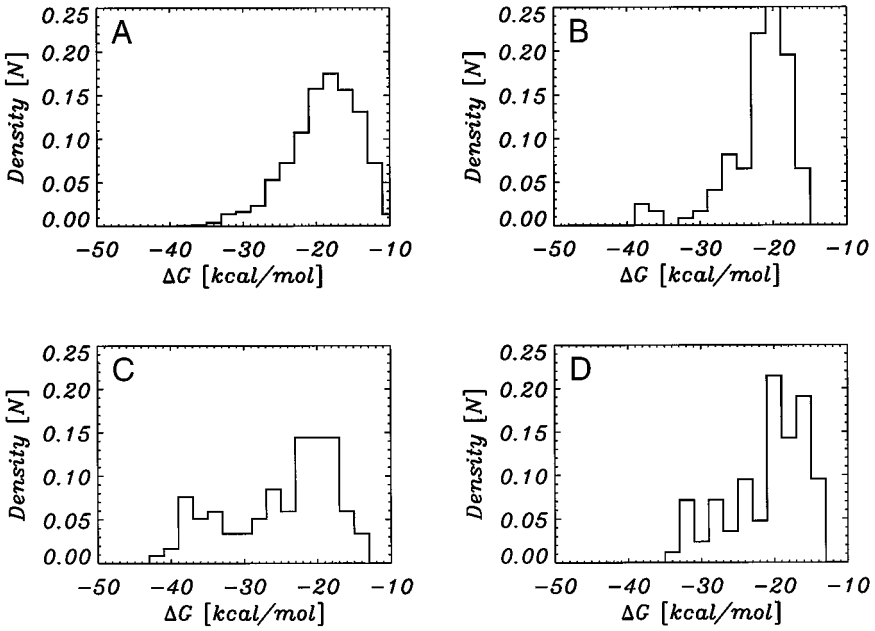

FIGURE 6 Population densities of label side chains versus energy, ΔG, determined by the systematic search procedure described in Materials and Methods. (*A*) IAEDANS, (*B*) BADAN, (*C*) IPSL, and (*D*) MTSSL. The bin size in the construction of the histograms is 1 kcal/mol.

complex (Banner et al., 1996; Zhang et al., 1999). sTF and FVIIa are essentially oriented side by side in the complex (Fig. 1), with FVIIa in an extended conformation. The contact surface involved in forming the sTF:FVIIa complex is extensive, 1810 $Å^2$ (Banner et al., 1996), and the energetic importance of individual contacts is thereby smaller than in more narrow binding sites. The Phe residue in position 140, the position selected for mutagenesis, is surface exposed in sTF but becomes buried when the complex is formed. The solvent exposure of F140, as determined from the crystal structures, changes from 62% to 20% upon sTF:FVIIa complex formation. In the region close to the mutation site (F140), the contact surface area between sTF and FVIIa involves mainly hydrophobic interactions (Banner et al., 1996), and F140 is reported to be a major contributor.

The F140C mutation had no detectable effect on the conformation of sTF as verified by CD measurements, and the cofactor function toward FVIIa was only moderately affected (Table 2). The small decrease in the ability of sTF(F140C) to allosterically activate FVIIa was of the same magnitude as has been reported for sTF(F140A) (Gibbs et al., 1994) and the labeling of sTF(F140C) with the labels used in this study had no further effect on the cofactor function (Table 2). The overall conformation of the labeled mutant also appeared to be intact, as judged from CD spectra. Thus, the minor impact on the function of labeled sTF(F140C) can be ascribed to the mutation per se and strongly indicates that the inserted labels can be accommodated in the sTF:FVIIa structure.

By probing the local environment of the spectroscopic labels attached to sTF(F140C) before and after complex formation with FVIIa, the sensitivity of the labels toward the protein-protein interaction was evaluated. Since sTF is known not to change conformation upon FVIIa association and the labeling of the sTF mutant does not disturb the 3D structure of the protein, any detectable spectral change can be assigned to the formation of the sTF:FVIIa complex.

In this study we have used two fluorescent labels (IAEDANS, BADAN) and two spin labels (IPSL, MTSSL) to monitor the interaction between sTF and FVIIa locally at position 140 in sTF (Fig. 1). A number of parameters were assigned as important for the probing performance: length, volume, flexibility, and polarity of the label. Both structural and physicochemical properties were found to vary considerably between the different labels (Table 3). Hence, it is likely that they will each probe the interaction between sTF(F140C) and FVIIa differently. Therefore, by using different labels a multitude of complementary information can be gained. Line-shape simulations of EPR spectra have been performed to obtain more details of the local dynamic structure surrounding the spin labels. These were improved by using g values and hyperfine splitting constants obtained from reference measurements in solvents similar to the environments which the spin labels are exposed to. We have also used molecular modeling techniques to generate possible orientations of the inserted labels at the site of mutation in the sTF:FVIIa complex. These modeled orientations are directly compared with the experimental data in order to rationalize the information from the spectroscopic measurements.

Fluorescence probing and modeling

The fluorescence spectra of IAEDANS- and BADAN-labeled sTF(F140C) are shown in Fig. 4, *A* and *B*. Both reveal a more apolar environment as the sTF:FVIIa complex is formed, which implies that we are capable of sensing the binding of the two molecules on a local level. It can be deduced from the wavelengths of the emission maxima of the spectra of the uncomplexed labeled sTF(F140C) that

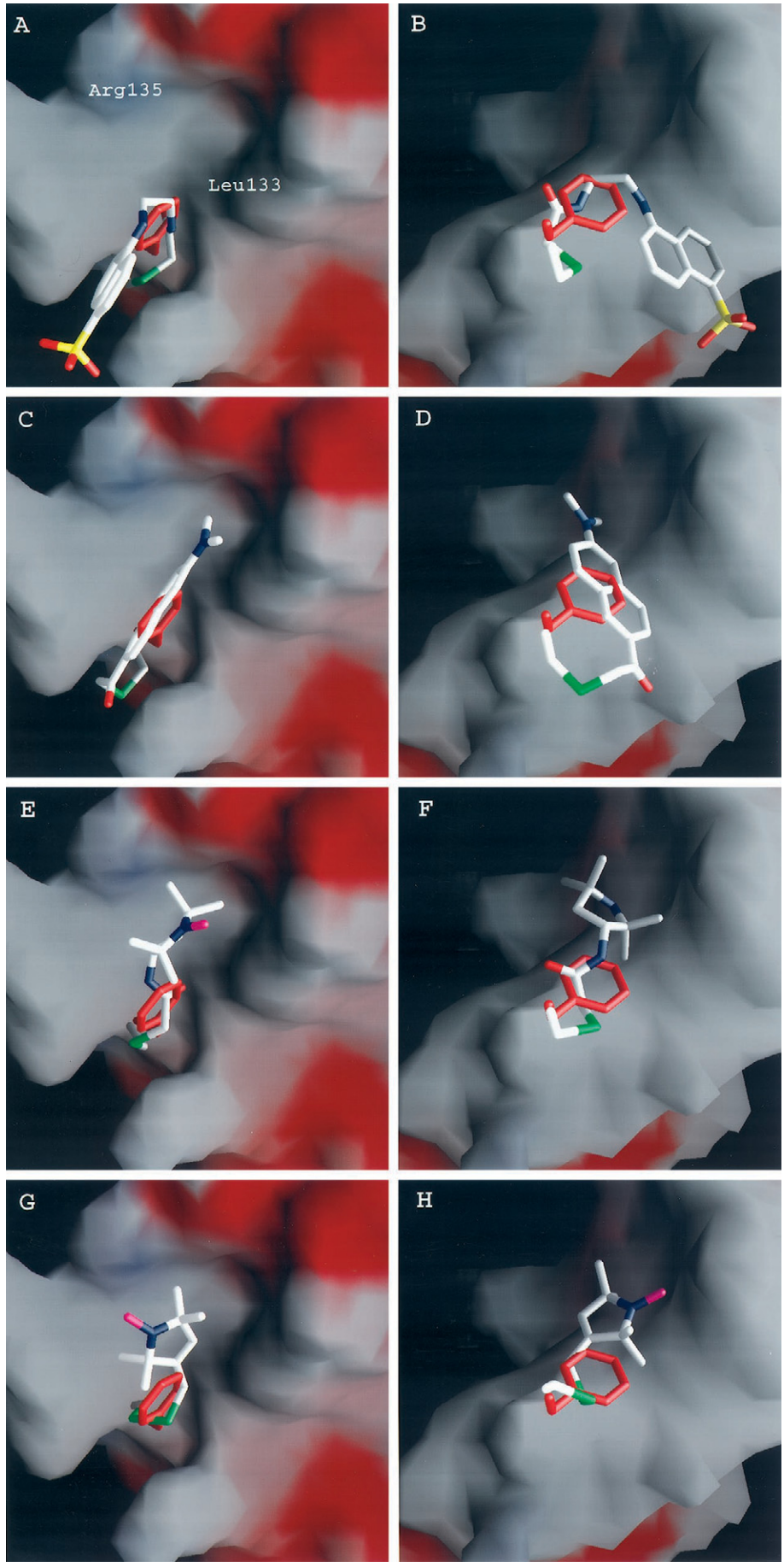

FIGURE 7 Structures of the lowest energy label side-chain conformations in complex with sTF:FVIIa found by the systematic search procedure described in Materials and Methods. (*A* and *B*) IAEDANS, (*C* and *D*) BADAN, (*E* and *F*) IPSL, and (*G* and *H*) MTSSL. Labels are shown in stick model and the proteins in a molecular surface model colored according to the electrostatic potential (*red/blue* correspond to negative/positive potential). The left figures show the labels interacting with sTF (FVIIa not shown), while the right figures (rotated 90°, i.e., opened up like a book about the vertical line, compared to the left figures) show the labels interacting with FVIIa (sTF not shown). The side chain of Phe-140 from the native sTF:FVIIa complex is shown in *red*. Figures are generated using the Grasp software (Nicholls et al., 1991).

both IAEDANS and BADAN sense some hydrophobic features (~20% EtOH) in their vicinity (Fig. 3). This is probably due to their ability to sense the surface of their host molecule (sTF(F140C)). The fluorescence quantum yield of IAEDANS-labeled sTF(F140C) is lower than that of IAEDANS-labeled β-mercaptoethanol, $\Phi_{rel} = 0.7$, and the fluorescence anisotropy is much smaller than what could be expected from a macromolecule of this size. These data indicate that the IAEDANS moiety has a considerable local mobility. Moreover, no ordered interaction between BADAN or IAEDANS and sTF was detected when searching for low-energy orientations of the inserted labels (data not shown). However, an examination of the positions generated in the uncomplexed form of sTF(F140C) shows a clustering around two regions on the surface of sTF, especially a hydrophobic patch around Leu-133. It is likely that the inserted labels are affected locally by the neighboring residues (especially Leu-133) in addition to being sequestered from surrounding water molecules. It is important to stress that these searches were performed without involving water molecules in the calculations.

As the sTF:FVIIa complex is formed, a ~10 nm blueshift is observed for both labeled variants corresponding to an environment of 45% EtOH (Fig. 3). Thus, the two labels seem to have the same ability to probe the sTF:FVIIa interaction. Still, IAEDANS shows a large increase in fluorescence intensity after complex formation, whereas BADAN does not (even though BADAN shows a large increase in the 45% EtOH environment (Fig. 3, *inset*)). This could be due to the location of some quencher group/groups in the vicinity of BADAN, which would imply that the two labels have different sensing areas. The molecular modeling data verify this hypothesis, as they suggest that the most energetically favorable orientation for each of the labels is significantly different (Fig. 7, *A–D*). The simulated structure for BADAN shows that Arg-135 in sTF is close to the dansyl ring, and since this residue is positively charged it can possibly act as a quencher. However, no potential quenchers are in close proximity to IAEDANS in the most favorable modeled orientation. Accordingly, the relative fluorescence quantum yield of IAEDANS-labeled sTF(F140C) in complex with FVIIa is close to one, i.e., it is not quenched by some neighboring group and shows an anisotropy that is not much affected by the local mobility of the label. However, IAEDANS might be quenched in the uncomplexed form of sTF, since the relative quantum yield for the IAEDANS labeled sTF(F140C) is 0.7, suggesting that the fluorophore is locally quenched by residues close to position 140. When the sTF:FVIIa complex is formed the IAEDANS moiety can be moved away from the quencher, obtaining a relative quantum yield close to that when coupled to β-mercaptoethanol.

EPR probing and modeling

The EPR spectra obtained from sTF(F140C) labeled with IPSL or MTSSL show that both labels are in a state of intermediate mobility (Fig. 5, *A* and *C*). Still, the low-field line of the sTF(F140C)-MTSSL spectrum is considerably broader compared to that of the sTF(F140C)-IPSL spectrum. This is due to the lower flexibility, smaller size, and/or hydrophobic properties of MTSSL, which makes it interact tighter with nearby residues of sTF(F140C) than IPSL does, resulting in a lower mobility. This is a good demonstration of the selectivity of the spin labels. The "kink" of the low-field line of the sTF(F140C)-MTSSL spectrum (Fig. 5 *C*) could not be reproduced in EPR simulations using a single component, indicating that the label resides in more than one distinct site. One explanation for this might be that the linker of IPSL is more flexible compared to the side chain of MTSSL, since in MTSSL there are only two energetically favored conformations available for the C_β-atoms linked to a disulfide bond (Richardson, 1981). Furthermore, a more flexible linker for IPSL is also supported by the results of the EPR line-shape simulations (Table 5). A much faster axial rotation and higher degree of rotational anisotropy were noted for IPSL ($d_{zz}/d_{xy} = 80$) compared to MTSSL ($d_{zz}/d_{xy} = 25$). Conclusively, in both cases the spin label is situated in a relatively hydrophobic environment with restricted ability to rotate about the linker arm. In addition, the generated orientations of the labels in sTF obtained from molecular modeling (not shown) show a subpopulation that favors an interaction in the same region where the fluorescent labels are clustered (around Leu-133). One can conclude from these data that the more restricted motion of the MTSSL spin label makes it more sensitive to the local environment than IPSL even though they are situated on the surface of a globular protein exposed to the solvent.

When the spin-labeled sTF(F140C):FVIIa complex is formed the EPR spectra obtained from both spin labels are dominated by anisotropic features and therefore show a substantial broadening (Fig. 5, *B* and *D*). A broadening of the EPR spectra was expected since the binding region between sTF and FVIIa in the vicinity of position 140 is dominated by hydrophobic interactions (Banner et al., 1996). However, the immobilization of the spin labels at position 140 when FVIIa binds to sTF is in fact equally or more pronounced compared to what we have observed when the labels are embedded in the hydrophobic interior of a protein (Lindgren et al., 1993, 1995; Svensson et al., 1995; Hammarström et al., unpublished results). Thus, it seems as though the hydrophobic interactions of the binding surface between sTF and FVIIa in this local area are at least as strong as in a large hydrophobic cluster within a globular protein. A factor contributing to this rigid position is certainly the suitable cavity for the spin labels in position 140 (Fig. 7, *E–H*). In the case of MTSSL-labeled sTF(F140C):FVIIa the anisotropic features of the EPR spectrum are close to those of a totally rigid spin label, which means that it must possess a location where it is interacting very strongly with neighboring residues at the protein interface. Interestingly, this labeled variant causes the greatest perturbation of the FVIIa activity (Table 2), which could be due

to its rigid conformation complicating adjustment to the surrounding structure during complex formation. A similar degree of immobilization of MTSSL has been reported recently in another receptor-ligand study (Klug et al., 1998). As in the case of uncomplexed sTF(F140C)-MTSSL, it is reasonable to believe that MTSSL finds this almost rigid position in the complex due to its constrained disulfide bond. This explanation is based upon the relatively minor difference in size and polar properties between the labels. The EPR spectrum obtained from MTSSL-labeled sTF(F140C):FVIIa could be simulated using one single component of rotational motion, describing only one rigid orientation for the label. IPSL, however, is clearly composed of at least two spectral components, indicating several more or less rigid orientations for the label.

The validity of the interpretations made from the spectral data and the properties of the labels were tested by modeling the most energetically favorable locations of the labels at position 140. These results indicate that both MTSSL and IPSL hold a position similar to the native Phe (Fig. 7, *E–H*). The energy of each generated structure of these spin labels (Fig. 6, *C* and *D*) shows that IPSL holds a larger subpopulation (between 40 and 30 kcal/mol) of structures than MTSSL (between 35 and 30 kcal/mol). This will allow IPSL to vibrate or rotate more easily than MTSSL, even though they occupy the same space and IPSL seems to possess a more stable conformation (Fig. 6, *C* and *D*). As discussed above the linker of IPSL is more flexible compared to the linker of MTSSL, allowing IPSL to adjust more freely to the surrounding environment. These observations indicate that similar labels respond differently, even though they occupy the same space in a protein, because of the chemical properties of the linker connecting the paramagnetic group to the backbone. Such an influence on the motion of spin labels has also been studied for spin-labeled T4 lysozyme (Mchaourab et al., 1999).

If we assume that the spectrum of MTSSL and the most rigid signature of IPSL is due to a tightly locked label between the two protein structures, the diffusion constant can be used to estimate the size and shape of the protein complex. Assuming spherically shaped particles, in a similar way as for the depolarization calculations, the theory of Brownian diffusion states the following relation between the diffusion constant and the radius, a, of the particle (protein) (Goldman et al., 1972):

$$\tau_R = \frac{1}{6R} = \frac{4\pi\eta a^3}{3kT} = \left(\frac{1}{6\sqrt{R_\perp R_\parallel}}\right)$$

where τ_R is the rotational correlation time, η the viscosity of the medium (here taken as water, $\eta = 0.001$ Ns/m^2), k the Boltzmann's constant, and T the temperature (20°C). Using the rotational diffusion constant (R) from line-shape simulations gives a radius of the MTSSL-labeled protein complex of 48 Å, whereas for the IPSL-labeled protein complex a radius of 21 Å is obtained. Considering the elongated shape of the protein complex, length = 115 Å, diameter = 40–50 Å (Banner et al., 1996), the "effective radius" calculated for all molecular probes is between the limits of the longest and shortest axes of an average ellipsoid structure (see Fig. 1).

The discrepancy between the two spin label cases can be explained if we take into account the anisotropy of the protein complex and a specific orientation of the spin label. When analyzing EPR spectra the anisotropic motion of the label will be more or less sensitive depending on the orientation of the rotating (diffusion) frame with respect to the static magnetic frame. Rotation about the z axis has little effect on the simulated spectral line-shape once the A_{xx}, A_{yy} and g_{xx}, g_{yy} components have been averaged out. Particularly the former is of nearly the same magnitude in nitroxide radicals. This means that if the MTSSL label is oriented within the protein complex with its magnetic z axis more parallel to the fast rotation axis of the protein, the line-shape simulations will be more sensitive to the perpendicular rotation parameter in the simulations. Line-shape simulations showed that this phenomenon can explain the discrepancy, since moderate increase of the d_{zz} parameter gave no dramatic effect on the simulated line-shape of MTSSL in Fig. 5 *D* (not shown).

A shorter "effective radius" for the IPSL label in the complex can also be explained by a more non-rigid environment surrounding the label. The more pronounced flexibility of the linker arm as indicated by the molecular modeling data support this interpretation.

In any case, one must be careful when estimating molecular radii from EPR spectra if there are two independent dynamic processes, one local and one global, especially if they are associated with similar rotational correlation times. The latter situation seems evident, particularly for IPSL.

CONCLUSIONS

In this study, we have been able to locally probe a protein-protein interaction by introducing spin and fluorescent labels that are capable of sensing a specific contact area in the large interface of the sTF:FVIIa system. Even though the fluorescent labels sense changes in polarity in their vicinity equally well, they describe the environment around position 140 in sTF(F140C) differently as the sTF(F140C):FVIIa complex is formed. Since the type of covalent bond of the fluorophores to the protein is the same, the discrepancy must be ascribed to different properties of the labels, such as size and lipophilicity, presumably resulting in different orientations of the labels in the complex as indicated by molecular modeling. Both spin labels were strongly immobilized in the sTF(F140C):FVIIa complex, but with a considerably lower tumbling rate for MTSSL compared to IPSL. Since the size and lipophilicity of the labels are almost equal, the difference in rotational motion is most likely caused by the higher constraint of the disulfide bond at the attachment site of MTSSL to sTF(F140C) and/or the smaller number of atoms in the linker of MTSSL. Accordingly, molecular modeling inferred a more restricted localization of the MTSSL label than that of the IPSL label, even though they occupy the same space in the protein structure.

Interestingly, the immobilization of the spin labels in the interface of the complex is equal to or even more pronounced than in a rigid hydrophobic core of a globular protein. By combining different spectroscopic techniques and labels, valuable complementary information regarding the characteristics of the vicinal structure can be extracted. Moreover, molecular modeling can be very useful in selecting appropriate labels for specific purposes.

We thank Dr. Björn Kalman for help with the evaluation of the fluorescence anisotropy measurements.

This work was supported by grants from Swedish Medical Research Council (to U.C., M.S.), Foundation for Strategic Research, and Swedish Natural Science Research Council (to U.C., M.L.).

REFERENCES

Banner, D. W., A. D'Arcy, C. Chène, F. K. Winkler, A. Guha, W. H. Konigsberg, Y. Nemerson, and D. Kirchhofer. 1996. The crystal structure of the complex of blood coagulation factor VIIa with soluble tissue factor. *Nature.* 380:41–46.

Brooks, B. R. III, R. E. Bruccoleri, B. D. Olafsen, D. J. States, S. Swaminthan, and M. Karplus. 1983. CHARMM: a program for macromolecular energy, minimization, and dynamics calculations. *J. Comp. Chem.* 4:187–217.

Cantor, C. R., and P. R. Schimmel. 1980. Biophysical Chemistry II: Techniques for the Study of Biological Structure and Function. W. H. Freeman and Company, San Francisco.

Connolly, M. L. 1983. Analytical molecular surface calculation. *J. Appl. Crystallogr.* 16:548–558.

Davie, E. W., K. Fujikawa, and W. Kisiel. 1991. The coagulation cascade: initiation, maintenance, and regulation. *Biochemistry.* 30:10363–10370.

Freskgård, P.-O., O. H. Olsen, and E. Persson. 1996. Structural changes in factor VIIa induced by Ca^{2+} and tissue factor studied using circular dichroism spectroscopy. *Protein Sci.* 5:1531–1540.

Gibbs, C. S., S. N. McCurdy, L. L. K. Leung, and L. R. Paborsky. 1994. Identification of the factor VIIa binding site on tissue factor by homologous loop swap and alanine scanning mutagenesis. *Biochemistry.* 33: 14003–14010.

Gill, S. C., and P. H. von. Hippel. 1989. Calculation of protein extinction coefficients from amino acid sequence data. *Anal. Biochem.* 182:319–326.

Goldman, S. A., G. V. Bruno, and J. H. Freed. 1972. Estimating slow-motional rotational times for nitroxides by electron spin resonance. *J. Phys. Chem.* 76:1858–1860.

Hammarström, P., B. Kalman, B.-H. Jonsson, and U. Carlsson. 1998. Pyrene excimer fluorescence as a proximity probe for investigation of residual structure in the unfolded state of human carbonic anhydrase II. *FEBS Lett.* 420:63–68.

Harlos, K., D. M. A. Martin, D. P. O'Brien, E. Y. Jones, D. I. Stuart, I. Polikarpov, A. Miller, E. G. D. Tuddenham, and C. W. G. Boys. 1994. Crystal structure of the extracellular region of human tissue factor. *Nature.* 370:662–666.

Heiden, W., G. Moeckel, and J. Brickmann. 1993. A new approach to analysis and display of local lipophilicity/hydrophilicity mapped on molecular surfaces. *J. Comp.-Aided Mol. Design.* 7:503–514.

Hubbell, W. L., A. Gross, R. Langen, and M. A. Lietzow. 1998. Recent advances in site-directed spin labeling of proteins. *Curr. Opin. Struct. Biol.* 8:649–656.

Kelley, R. F., K. E. Costas, M. P. O'Connell, and R. A. Lazarus. 1995. Analysis of the factor VIIa binding site on human tissue factor: effects of tissue factor mutations on the kinetics and thermodynamics of binding. *Biochemistry.* 34:10383–10392.

Klug, C. S., S. S. Eaton, G. R. Eaton, and J. B. Feix. 1998. Ligand-induced conformational change in the ferric enterobactin receptor FepA as studied by site-directed spin labeling and time-domain ESR. *Biochemistry.* 37:9016–9023.

Likhtenshtein, G. I. 1993. Biophysical Labeling Methods in Molecular Biology. Cambridge University Press, New York.

Lindgren, M., M. Svensson, P.-O. Freskgård, U. Carlsson, B.-H. Jonsson, L.-G. Mårtensson, and P. Jonasson. 1993. Probing local mobility in carbonic anhydrase: EPR of spin-labelled SH groups introduced by site-directed mutagenesis. *J. Chem. Soc., Perkin Trans.* 2:2003–2008.

Lindgren, M., M. Svensson, P.-O. Freskgård, U. Carlsson, P. Jonasson, L.-G. Mårtensson, and B.-H. Jonsson. 1995. Characterization of a folding intermediate of human carbonic anhydrase II: Probing local mobility by electron paramagnetic resonance. *Biophys. J.* 69:202–213.

Mann, K. G., M. E. Nesheim, W. R. Church, P. Haley, and S. Krishnaswamy. 1990. Surface-dependent reactions of the vitamin K-dependent enzyme complexes. *Blood.* 76:1–16.

Mchaourab, H. S., T. Kálai, K. Hideg, and W. L. Hubbell. 1999. Motion of spin-labeled side chains in T4 Lysozyme: effect of side chain structure. *Biochemistry.* 38:2947–2955.

Muller, Y. A., M. H. Ultsch, R. F. Kelley, and A. M. d. Vos. 1994. Structure of the extracellular domain of human tissue factor: location of the factor VIIa binding site. *Biochemistry.* 33:10864–10870.

Muller, Y. A., M. H. Ultsch, and A. M. d. Vos. 1996. The crystal structure of the extracellular domain of human tissue factor refined to 1.7 Å resolution. *J. Mol. Biol.* 256:144–159.

Nicholls, A., K. Sharp, and B. Honig. 1991. Protein folding and association: insights from the interfacial and thermodynamic properties of hydrocarbons. *Proteins: Struct., Funct., Genet.* 11:281–296.

Persson, M., P. Hammarström, M. Lindgren, B.-H. Jonsson, M. Svensson, and U. Carlsson. 1999. EPR mapping of interactions between spin-labeled variants of human carbonic anhydrase II and GroEL: evidence for increased flexibility of the hydrophobic core by the interaction. *Biochemistry.* 38:432–441.

Persson, E., O. H. Olsen, A. Østergaard, and L. S. Nielsen. 1997. Ca^{2+} binding to the first epidermal growth factor-like domain of factor VIIa increases amidolytic activity and tissue factor affinity. *J. Biol. Chem.* 272:19919–19924.

Richardson, J. S. 1981. The anatomy and taxonomy of protein structure. *Adv. Protein Chem.* 34:167–339.

Riddles, P. W., R. L. Blakely, and B. Zerner. 1983. Reassessment of Ellman's reagent. *Methods Enzymol.* 91:49–60.

Ruf, W., C. R. Kelly, J. R. Schullek, D. M. A. Martin, I. Polikarpov, C. W. G. Boys, E. G. D. Tuddenham, and T. S. Edgington. 1995. Energetic contributions and topographical organization of ligand binding residues of tissue factor. *Biochemistry.* 34:6310–6315.

Ruf, W., J. R. Schullek, M. J. Stone, and T. S. Edgington. 1994. Mutational mapping of functional residues in tissue factor: identification of factor VII determinants in both structural modules of the predicted cytokine receptor homology domain. *Biochemistry.* 33:1565–1572.

Schneider, D. J., and J. H. Freed. 1989. Calculating slow motional magnetic resonance spectra. *In* Biological Magnetic Resonance, Vol. 8: Spin Labeling—Theory and Applications. L. J. Berliner and J. Reuben, editors. Plenum Press, New York. 1–76.

Schullek, J. R., W. Ruf, and T. S. Edgington. 1994. Key ligand interface residues in tissue factor contribute independently to factor VIIa binding. *J. Biol. Chem.* 269:19399–19403.

Stone, M. J., W. Ruf, D. J. Miles, T. S. Edgington, and P. E. Wright. 1995. Recombinant soluble human tissue factor secreted by *Saccharomyces cerevisiae* and refolded from *Escherichia coli* inclusion bodies: glycosylation of mutants, activity and physical characterization. *Biochem. J.* 310:605–614.

Svensson, M., P. Jonasson, P.-O. Freskgård, B.-H. Jonsson, M. Lindgren, L.-G. Mårtensson, M. Gentile, K. Borén, and U. Carlsson. 1995. Mapping the folding intermediate of human carbonic anhydrase II. Probing substructure by chemical reactivity and spin and fluorescence labeling of engineered cysteine residues. *Biochemistry.* 34:8606–8620.

Thim, L., S. Bjoern, M. Christensen, E. M. Nicolaisen, T. Lund-Hansen, A. H. Pedersen, and U. Hedner. 1988. Amino acid sequence and post-translational modifications of human factor VIIa from plasma and transfected baby hamster kidney cells. *Biochemistry.* 27:7785–7793.

Zhang, E., R. St. Charles, and A. Tulinsky. 1999. Structure of extracellular tissue factor complexed with factor VIIa inhibited with a BPTI mutant. *J. Mol. Biol.* 285:2089–2104.